Sliding Mode Control of PMSG Wind Turbine Based on Enhanced Exponential Reaching Law

Seyed Mehdi Mozayan, Maarouf Saad, *Senior Member*, *IEEE*, Hani Vahedi, *Student Member*, *IEEE*, Handy Fortin-Blanchette, *Member*, *IEEE* and Mohsen Soltani, *Member*, *IEEE*

***Abstract*—This paper proposes a Sliding Mode Control (SMC) based scheme for a variable speed, direct-driven Wind Energy Conversion Systems (WECS) equipped with Permanent Magnet Synchronous Generator (PMSG) connected to the grid. In this work, diode rectifier, boost converter, Neutral Point Clamped (NPC) inverter and L filter are used as the interface between the wind turbine and grid. This topology has abundant features such as simplicity for low and medium power wind turbine applications. It is also less costly than back-to-back two-level converters in medium power applications. SMC approach demonstrates great performance in complicated nonlinear systems control such as WECS. The proposed control strategy modifies Reaching Law (RL) of sliding mode technique to reduce chattering issue and to improve THD property compared to conventional reaching law SMC. The effectiveness of the proposed control strategy is explored by simulation study on a 4 kW wind turbine, and then verified by experimental tests for a 2 kW set-up.**

***Index Terms*—Wind Turbine, Permanent Magnet Synchronous Generator (PMSG), Boost Converter, Neutral Point Clamped (NPC), Sliding Mode Control (SMC), Enhanced Exponential Reaching Law (EERL), Generator Control, Converter Control.**

I. Introduction

RENEWABLE energy has been considered as an alternative energy source because fossil fuels are limited and make pollution problems. Renewable energy integration in power system raises a lot of challenges in research and practice [1], [2]. One of the most favorable sources of renewable energy technology is Wind Energy Conversion System (WECS) technology. This technology has been improved from the capacity of few tens of kilo Watts to several mega Watts over the past few decades [3]. Worldwide investment in WECS area is going to be expanded in the future [4]. Today, WECSs equipped with Permanent Magnet Synchronous Generator (PMSG) are becoming more popular in wind energy community, especially in offshore applications due to the elimination of gear box and excitation system [5].

Manuscript received September 21, 2015; revised December 22, 2015, February 11, 2016, and March 15, 2016; accepted March 31, 2016.

S. M. Mozayan, M. Saad, H. Vahedi and H. Fortine-Blanchette are with the Department of Electrical Engineering, ÉTS, University of Quebec, Montreal, QC H3C 1K3, Canada. (seyed-mehdi.mozayan.1@ens.etsmtl.ca; maarouf.saad@etsmtl.ca; hani.vahedi@etsmtl.ca; handy.fortin-blanchette@etsmtl.ca).

M. Soltani is with the Department of Energy Technology, Aalborg University, Niels Bohrs Vej 8, 6700 Esbjerg, Denmark (sms@et.aau.dk).

In PMSG based WECS, the generator is directly connected to the electrical network through a power converter. Various power electronic converter topologies have been proposed to engage in wind turbine applications. Among these topologies, multilevel converters such as Neutral Point Clamped (NPC) converter are gaining prominence to play an interface role in grid-tied applications because it outputs more voltage level while having less switch stress [6], [7]. These advantages of NPC converter make it promising to transfer the electrical energy at low to medium voltage with lower current, less paralleled devices, and reduced size of filter in comparison with two-level converter [8], [9]. Topologies including diode rectifier and boost converter are also of great interest to join the PMSG to DC link [10]–[13]. Nonetheless, the integration of megawatt range wind turbines with advanced power electronic converters to the power grid is bringing new problems associated with voltage and frequency control of Point of Common Coupling (PCC).

Most studies in the field of WECS are dedicated to the development of appropriate control techniques to increase its ability to supply and regulate active and reactive power in both grid connected and islanding modes [14]. Several control approaches have been applied for PMSG based WECS control to reduce generator currents, to extract maximum power from wind turbine, to keep DC link voltage constant, to control the reactive power injected to the grid, and to decrease current harmonics at PCC. These control strategies of PMSG wind turbines can be generally arranged into two categories [15]. In the first category, Maximum Power Point Tracking (MPPT) is achieved by Machine Side Converter (MSC) control, whereas the DC link voltage is governed by Grid Side Converter (GSC) control [16]–[18]. In the second one, GSC adjusts the active power extraction from wind turbine, and the DC link voltage control is obtained by MSC control [19].

In both cases, vector control is applied to achieve control objectives. Different control schemes have been developed to achieve the control objectives of PMSG based WECS operation. Three prevalent methods being used to achieve the control goals are: Zero d-Axis Current (ZDC) control, Maximum Torque per Ampere (MTPA) control, and Unity Power Factor (UPF) control [20].

Researchers have adopted different linear control schemes to control grid-connected inverter [21], [22]. However, these solutions have main disadvantages such as: incapability to track sinusoidal trajectory references and poor capability to reject system disturbance. Generally, most of linear approaches

have the ability to meet some of the operation necessities [23]. Several studies have been conducted focusing on nonlinear techniques to control grid-tied PMSG [24], [25]. These methods are sensitive to modeling errors, difficult to implement, and require the exact PMSG parameters [26], [27]. On the other hand, SMC method as one of the control approaches in both linear and nonlinear systems, has gained a lot of attention due to its robustness, order reduction, insensitivity to parameter variations, finite time convergence, disturbance rejection, good dynamic behavior, and simple implementation [28], [29].

The main drawback of SMC is the chattering phenomenon because of discontinuous function in SMC. Many approaches have been proposed to eliminate or attenuate chattering issue which is undesirable in some applications [23], [30], [31]. An interesting method to reduce chattering phenomenon is to use Adjustable Reaching Law (ARL) instead of having a Constant Reaching Law (CRL) gain in SMC [30], [32]. A kind of ARL based on applying an exponential term in the reaching law was proposed in [30] which improves chattering reduction aspect of the controller but it can be further improved in some aspects to be applied in power electronics applications such as Total Harmonic Distortion (THD)improvement of grid current at PCC.

Proposed ARL sliding mode technique in this research performs the controller gain correction based upon the discrepancy between the actual and desired system states (error signal). When the error value is high, the gain is increased such that to force the system state to move toward the desired state as fast as possible. When the error signal becomes small, the applied gain is going to decrease in a way that once the gain tends to zero, the error inclines to zero. It is worth noting that the ARL approaches suggested in the literature do not amend the gain in a wise manner in the wide range of error values from zero to high error quantities. Therefore, the proposed approach in this paper is more pragmatic than the methods proposed in [30], [32].

In this paper, our scope is to propose an SMC based controller, called Enhanced Exponential Reaching Law (EERL) sliding mode approach which can meet the requirements in power applications. The contributions of the paper are three folds: First, EERL reduces the reaching time of system trajectory to the equilibrium point even the initial condition of the system parameters are far from the sliding surface. Second, EERL has the capability to further mitigate chattering issue of sliding mode approach with respect to the conventional SMC. Then, EERL improves current THD of the grid-connected inverter which is vital for Distributed Generation (DG) integration into the power grid. In this study, power control of PMSG is carried out by boost converter and UPF method is applied for NPC inverter control.

This paper is structured as follows. A brief review of SMC theory and EERL is presented in section II. In section III, modeling of PMSG wind turbine and its components are explained. Proposed control scheme based on sliding mode approach is described and applied in section IV. Numerical simulation and experimental results are reported in section V. Finally, section VI concludes the summary of key features of the proposed controller.

II. Sliding mode control theory based on modified reaching law

Mathematical model of real plants are always imprecise. This mismatch can be generated due to parametric uncertainties and unmodeled dynamics. Thus a control system is needed to be robust to these inaccuracies to have the strength of keeping the system performance stable. Sliding mode control is a powerful robust control method for uncertain systems that has been widely researched in both theoretical and industrial application aspects. The general concept of SMC theory is explained in [33]. As a motivation to overcome aforementioned limitations, a new reaching law, EERL, will be presented and formulated. Intuitively, SMC methodology replaces n^{th} order system by a 1^{st} order system which can be controlled easily by choosing a well-mannered function of the tracking error called sliding surface or sliding manifold. It moves the system trajectory from its initial point to the sliding manifold in finite time, and then constrains the variables such that to lie within a vicinity of the sliding surface by a control law. For illustration purposes of SMC theory, a second order nonlinear system with following state equation is considered

$$\ddot{x} = f(x, \dot{x}) + g(x, \dot{x})u, \tag{1}$$

where x and u are state and input vectors; and f and g are bounded nonlinear matrix functions of the system states. It is supposed that function g is continuous and invertible. The control aim is to get the state vector to track the desired state vector in the presence of disturbances and uncertainties. Let $\widetilde{x} = x - x_d$ be the trajectory error in state vector x, where x_d is desired state vector. Conventionally, time-varying sliding surface for a n^{th} order system is chosen as

$$S(t) = (\frac{d}{dt} + \Lambda)^{n-1}(x - x_d), \tag{2}$$

where Λ is a strictly positive number. For second order systems, one can define following surface

$$S(t) = \Lambda\widetilde{x} + \dot{\widetilde{x}}. \tag{3}$$

Therefore, the problem of tracking the desired vector is equivalent to keeping S at zero all the times. In fact, there are two different modes in SMC methodology. In reaching stage, tracking error vector $\widetilde{x}$ is reached to the sliding surface $S = 0$ in a finite time. Since sliding surface is an invariant set, system trajectory slides and remains on $S = 0$ in sliding stage. It is worth mentioning that S can be selected as $x - x_d$ for first order systems.

The problem of keeping the error vector on the sliding surface can be obtained by defining the control law u such that

$$\frac{1}{2}\frac{d}{dt}S^2 \leq -\eta\,|S|\,, \tag{4}$$

where η is a strictly positive constant. Satisfying above condition keeps the system trajectories remaining on the sliding surface. Sliding condition (4) can be expressed as

$$S\dot{S} \leq 0. \tag{5}$$

Integrating Eq. (4) results in

$$t_{reach} \leq |S(t=0)|/\eta, \tag{6}$$

where t_{reach}, reaching time, is the required time for $\widetilde{x}$ to reach the sliding surface. With the purpose of satisfying expression (5), $\dot{S}$ is generally taken as

$$\dot{S} = -Ksign(S), \tag{7}$$

where $sign$ is the sign function and K is also a positive constant. Choosing K large enough guarantees sliding condition in constant rate reaching law SMC. To satisfy sliding condition despite uncertainty in the system, a discontinuous term can be added to control input. Accordingly our control input takes the form

$$u = u_{con} + u_{discon}. \tag{8}$$

Therefore, it is as follows

$$u = g^{-1}(-f + \ddot{x}_d - \Lambda\widetilde{x} - Ksign(S)). \tag{9}$$

It is obvious that control law is composed of two terms. Discontinuous term which is applied due to imprecision of system modeling and disturbances, leads to an undesired phenomenon called chattering. Chattering might stimulate ignored high frequency dynamics of the system model. Choosing appropriate value of K would be a trade-off between reaching time and level of chattering. This method is called CRL sliding mode approach. Several works are done to attenuate or eliminate the chattering issue by modifying reaching law. In [32], they proposed constant-proportional rate reaching law and power rate reaching law. Constant-proportional rate reaching law has the form

$$\dot{S} = -\Lambda S - Ksign(S). \tag{10}$$

Definite integration of (10) between zero and t_{reach} leads to

$$\int_{S(t=0)=S_0}^{S(t_{reach})} \frac{dS}{\Lambda S + Ksign(S)} = \int_0^{t_{reach}} -dt. \tag{11}$$

Note that $S(t_{reach}) = 0$. For $S \geq 0$, reaching time is

$$t_{reach} = \frac{1}{\Lambda} ln \frac{\Lambda S_0 + K}{K}. \tag{12}$$

If $S \leq 0$, it yields

$$t_{reach} = \frac{1}{\Lambda} ln \frac{-\Lambda S_0 + K}{K}. \tag{13}$$

Therefore, one can simply express the reaching time in all conditions as

$$t_{reach} = \frac{1}{\Lambda} ln \frac{\Lambda |S_0| + K}{K}. \tag{14}$$

The main disadvantage of (10) is that reaching law is not adjustable. Power rate reaching scheme is as

$$\dot{S} = -K|S|^{\gamma_x} sign(S), \tag{15}$$

where $0 < \gamma_x < 1$ and $K > 0$. By applying the same procedure as explained before, the reaching time is as

$$t_{reach} = \frac{1}{(1-\gamma_x)K} |S_0|^{(1-\gamma_x)}. \tag{16}$$

The demerit feature of (15) is the reduction of its robustness due to the rapid lessening of the exponential term $|S|^{\gamma}$. In [30], an additional term is introduced to reduce chattering problem in robot applications by defining following function to handle reaching law

$$\dot{S} = -\frac{K}{D(S)} sign(S), \tag{17}$$

where

$$D(S) = \alpha + (1-\alpha)e^{-\beta_x |S|}. \tag{18}$$

In Eq. (18), $0 < \alpha < 1$ and $\beta_x > 0$. This method is called Exponential Reaching Law (ERL) approach. The reaching time for ERL is obtained as

$$t_{reach} = \frac{1}{K}(\alpha |S_0| + \frac{(1-\alpha)}{\beta_x}[1 - e^{-\beta_x |S_0|}]). \tag{19}$$

This method brings a lot of advantages such as gain adaptation based on the position of S_0 regarding the sliding surface, smaller reaching time and chattering reduction but shows a higher THD than our proposed method which might cause problem in power electronics application.

To solve above mentioned issues, an EERL is applied which is a combination of different concepts in [30] and [32] as well as applying new structure for managing the reaching law in both reaching and sliding stages. Our proposed EERL is as follows

$$\dot{S} = -\Lambda S - \frac{K}{D(S)} |S|^{\gamma_x} sign(S). \tag{20}$$

It is obvious if α tends to 1, proposed EERL is converted to power rate reaching law. Note that $D(S)$ is strictly positive at all time, therefore it does not have any impact on the SMC approach stability. In the proposed EERL, if $|S|$ raises, D(S) goes towards α, then coefficient of sign function would be $K|S|^{\gamma_x}/\alpha$. In contrast, when $|S|$ reduces, it tends to $K|S|^{\gamma_x}$. This phenomenon makes the controller gain to be modified between $K|S|^{\gamma_x}$ and $K|S|^{\gamma_x}/\alpha$; therefore, it adjusts the reaching time to approach to the sliding surface. In other words, EERL approach specifies faster reaching speed or smaller reaching time with respect to the constant rate reaching law SMC considering similar gain K. In addition, existence of Λ and γ_x along with $D(S)$ simultaneously in the controller will augment the characteristics of the controller while eliminating the disadvantages of each approach.

Fig. 1 illustrates the effect of the coefficient of sign function using the methods explained before. From Fig. 1, one can see that when $|S|$ is small, coefficient of sign function in methods ERL and EERL are approximately the same. On the contrary, when $|S|$ increases, coefficient in EERL concept becomes bigger than coefficient in ERL approach. It signifies that attraction of system trajectory to the sliding surface in

This article has been accepted for publication in a future issue of this journal, but has not been fully edited. Content may change prior to final publication. Citation information: DOI 10.1109/TIE.2016.2570718, IEEE Transactions on Industrial Electronics

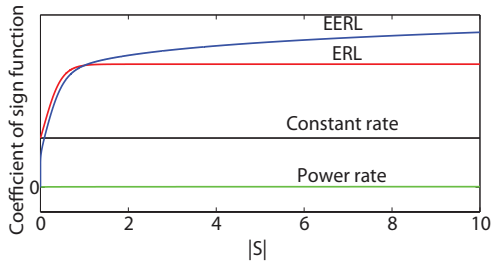

Fig. 1. Sign coefficient comparison based upon different sliding mode control methods.

EERL in high $|S|$ is faster than ERL. When the system state comes closer to the sliding surface, coefficients of both ERL and EERL methods gently diminish to mitigate the chattering problem. This figure explicitly exhibits that the gain of EERL decrease a lot when $|S|$ is extremely small, while in ERL the gain will approach K when $|S|$ is even near zero. Hereupon, the gain of EERL is altered elaborately to span the whole range of error vector $\widetilde{x}$, no matter how big or small the error is. Consequently, EERL method manipulates the system states more suitable than ERL whenever $|S|$ is very high or very small. Fig. 1 also indicates that sign coefficient associated with power rate approach would be always near zero when γ is chosen small. Moreover, constant rate approach provides constant coefficient all the time.

III. Dynamic Model of the PMSG Based Wind Turbine

This section briefly explains elements of the system and provides their governing equations. Fig. 2 demonstrates the general overview of grid connected PMSG based WECS. The aerodynamic torque made by forces acting on the blades is transferred to PMSG via the drive train. Then PMSG converts the mechanical energy into electrical energy. This energy is injected to the grid through diode rectifier, boost converter, NPC inverter and L filter to meet the required objectives. This topology is used in both low and medium voltage applications [3], [34], [35] and [36]. The advantages of this scheme are: simple control and system cost reduction [20].

The theoretically available power in the wind can be stated as

$$P_{available} = \frac{1}{2}\rho A v_w^3, \tag{21}$$

where ρ, v and A are the air density (kg/m^3), the wind speed (m/s) and the swept area of rotor blades (m^2), respectively. Due to physical limits, wind turbine blades only transfer portion of the wind kinetic energy. The absorbed mechanical power by rotor is given by the following expression

$$P_t = \frac{1}{2}\pi\rho R^2 v_w^3 C_p(\lambda,\beta), \tag{22}$$

where C_p is power coefficient. In WECS aerodynamics, there are two main variables that make C_p change: blade pitch angle β and tip speed ratio (TSR) of the blade $\lambda = R\omega_{rm}/v_\omega$ in which R and ω_{rm} are the rotor plane radius and the angular velocity of the rotor, respectively.

In the literature, models with different level of complexity are available for the drive train subsystem. The available drive train models of the WECS are six-mass model, three-mass model, two-mass model and one-mass (lumped) mode [37]. One-mass model is chosen in this paper to simplify state space model of the system.

The generation capacity of a WECS is usually specified by a curve based on the generator output power versus actual wind speed which is called WECS power curve. The wind speed operational range in WECS is between the cut-in ($v_{\omega-min}$) and cut-out ($v_{\omega-max}$) wind speeds. In the wind speeds lower than $v_{\omega-min}$ and higher than $v_{\omega-max}$ (regions I, IV), the wind turbine system is shut down (or may spin freely in region I). The WECS operation can be described in four different regions based on the wind speed. At wind speeds between $v_{\omega-min}$ and nominal speed (region II), the available wind power would be lower than generator rated power. So, the generation goal in this operation region is to capture maximum power. Hence, the extracted power in this region is calculated by

$$P_t = \frac{1}{2}\pi\rho R^2 v_w^3 C_{p-max}. \tag{23}$$

In the wind speed higher than rated wind speed value and lower than $v_{\omega-max}$ (region III), the WECS power curve remains constant at rated power. Therefore the wind turbine must operate with power coefficients lower than C_{p-max}. Fig. 3 demonstrates power curve of a typical wind turbine in which working regions are explicitly shown.

To investigate wind turbine dynamic behavior, it is necessary to model other components of the WECS. Dynamic model of the surface mounted PMSG in dq rotor reference frame is well-studied in the literature [12], [15] and [31].

To model boost converter, following equations are used

$$\frac{dI_{dc}}{dt} = -\frac{R_{dc}}{L_{dc}}I_{dc} + \frac{1}{L_{dc}}V_r - \frac{(1-q)}{L_{dc}}V_{dc}, \tag{24}$$

$$\frac{dV_r}{dt} = \frac{1}{C_0}I_r - \frac{1}{C_0}I_{dc}, \tag{25}$$

where R_{dc} and L_{dc} are resistance and inductance of boost converter, V_r and I_r are the rectifier output voltage and current, V_{dc} is the DC link voltage, $0 \le q \le 1$ is the duty cycle used for generation of switching signal, and I_{dc} is the inductor current. It must be mentioned that V_{dc} as a system state is controlled by grid currents in our study.

The equations of L filter in synchronous reference frame are as

$$\frac{di_{dg}}{dt} = -\frac{R_f}{L_f}i_{dg} + \frac{1}{L_f}v_{di} - \frac{1}{L_f}v_{dg} + \omega_g i_{qg}, \tag{26}$$

$$\frac{di_{qg}}{dt} = -\frac{R_f}{L_f}i_{qg} + \frac{1}{L_f}v_{qi} - \frac{1}{L_f}v_{qg} - \omega_g i_{dg}, \tag{27}$$

where R_f and L_f are resistance and inductance of the filter, v_{dg} and v_{qg} are grid voltages, v_{di} and v_{qi} are NPC inverter output voltages, di_{dg} and di_{qg} are grid currents, and ω_g is the grid angular velocity.

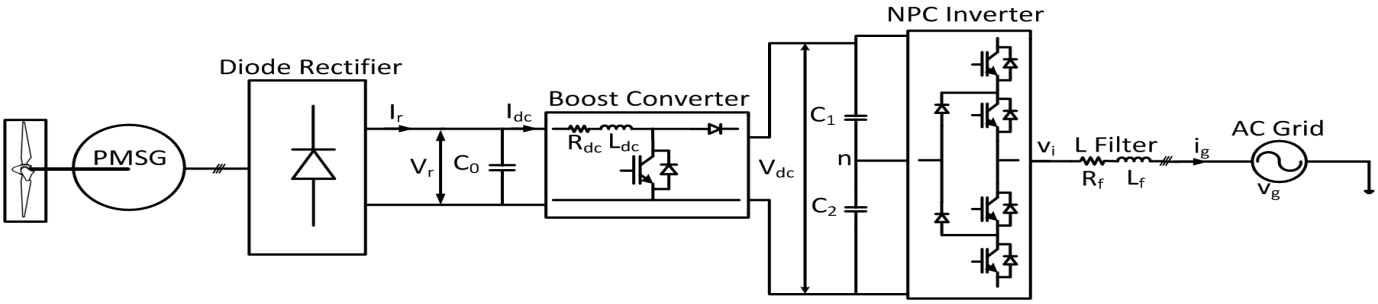

Fig. 2. General overview of grid connected PMSG.

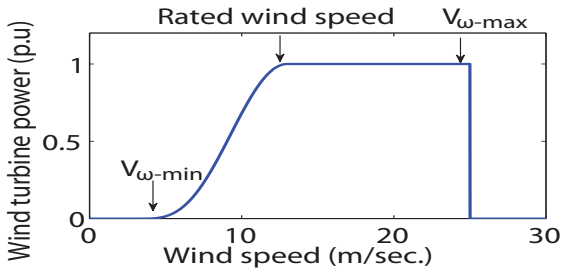

Fig. 3. Typical power curve of wind turbine systems.

IV. Controller Design for PMSG Wind Turbine

In order to control PMSG based WECS, it is required to generate appropriate switching signals for boost converter and NPC inverter based on the PMSG parameters and connection point requirements. Our proposed sliding mode controller based on EERL considering the first order dynamics has the following structure

$$u = g^{-1}(-f + \dot{x}_d - \Lambda S - \frac{K}{D(S)}|S|^{\gamma_x} sign(S)). \quad (28)$$

This expression can be applied to every system with governing equation similar to (1), considering the availability of inverse of g function. Noticeably, there exists inverse functions of the above-mentioned equations of PMSG based WECS components. It is employed to generate duty cycles for boost converter and NPC inverter switches. Based on Fig. 2, essential input and state vectors are as follows

$$x = \begin{bmatrix} V_r & I_{dc} & V_{dc} & i_{dg} & i_{qg} \end{bmatrix}^T, \quad (29)$$

$$u = \begin{bmatrix} q & v_{di} & v_{qi} \end{bmatrix}^T, \quad (30)$$

where superscript T indicates transposition of the matrix.

As diode rectifier is not a controllable converter, generated power by PMSG can be controlled by I_{dc} [38]. To control boost converter, Eq. (25) is considered. Based on EERL sliding approach, the final control input is as

$$\begin{aligned} q = & -\frac{R_{dc}}{V_{dc}} i_{dc} + \frac{(V_{dc} - V_{dc0})}{V_{dc}} + \frac{L_{dc}}{V_{dc}} \frac{di_{dc-ref}}{dt} \\ & - \frac{L_{dc}}{V_{dc}} \Lambda_{dc} S_{dc} - \frac{L_{dc}}{V_{dc}} \frac{K_{dc}}{D_{dc}(S_{dc})} |S_{dc}|^{\gamma_{dc}} sign(S_{dc}), \end{aligned} \quad (31)$$

where $S_{dc} = i_{dc} - i_{dc-ref}$ and $D_{dc}(S_{dc}) = \alpha_{dc} + (1 - \alpha_{dc})e^{-\beta_{dc}|S_{dc}|}$. In (31), V_{dc} has to be controlled such that it is a constant voltage. Desired current of L_{dc} is obtained by MPPT scheme of PMSG. Various MPPT algorithms for PMSG based WECS have been proposed. In this paper, TSR control is chosen for the MPPT algorithm in which ω_{rm-ref} is obtained using $v_w \lambda_{opt}/R$. Optimum value of TSR is the point that maximizes power coefficient. Commonly, following generic expression is used to model the WECS efficiency for extracting mechanical energy from wind kinetic energy [39]

$$C_p(\beta, \lambda) = c_1(\frac{c_2}{\lambda_i} - c_3\beta - c_4\beta^x - c_5)e^{-c_6/\lambda_i} + c_7\lambda, \quad (32)$$

with

$$\frac{1}{\lambda_i} = \frac{1}{(\lambda + 0.08\beta)} - \frac{0.035}{\beta^3 + 1}, \quad (33)$$

where the coefficients c_1 through c_7 and x are just the C_p curve fitting coefficients. Consequently, boost converter control diagram method is depicted in Fig. 4(a).

To control NPC inverter, our goal is to obtain unity power factor for grid-tied inverter. Hence, quadrature current injected to grid is set to be zero. Considering the L filter state space Eqs. (26) and (27), the control signals in dq reference frame are expressed as

$$\begin{aligned} v_{di} = & R_f i_{dg} - L_f \omega_g i_{qg} + v_{dg} + L_f \frac{di_{dg-ref}}{dt} \\ & - L_f \Lambda_d S_d - L_f \frac{K_d}{D_d(S_d)} |S_d|^{\gamma} sign(S_d), \end{aligned} \quad (34)$$

$$\begin{aligned} v_{qi} = & R_f i_{qg} + L_f \omega_g i_{dg} + v_{qg} + L_f \frac{di_{qg-ref}}{dt} \\ & - L_f \Lambda_q S_q - L_f \frac{K_q}{D_q(S_q)} |S_q|^{\gamma} sign(S_q), \end{aligned} \quad (35)$$

where $S_d = i_{dg} - i_{dg-ref}$, $S_q = i_{qg} - i_{qg-ref}$, $D_d(S_d) = \alpha_d + (1 - \alpha_d)e^{-\beta_d|S_d|}$ and $D_q(S_q) = \alpha_q + (1 - \alpha_q)e^{-\beta_q|S_q|}$. NPC control approach is shown in Fig. 4(b).

If we suppose that quadrature component of grid voltage, v_{qg} is equal to zero, and also having unity power factor $i_{qg} = 0$, then active and reactive power injected to the grid based on synchronous dq reference frame are $\frac{3}{2} v_{dg} i_{dg}$ and 0 respectively. Therefore, direct and quadrature components control of grid current leads to active and reactive power

This article has been accepted for publication in a future issue of this journal, but has not been fully edited. Content may change prior to final publication. Citation information: DOI 10.1109/TIE.2016.2570718, IEEE Transactions on Industrial Electronics

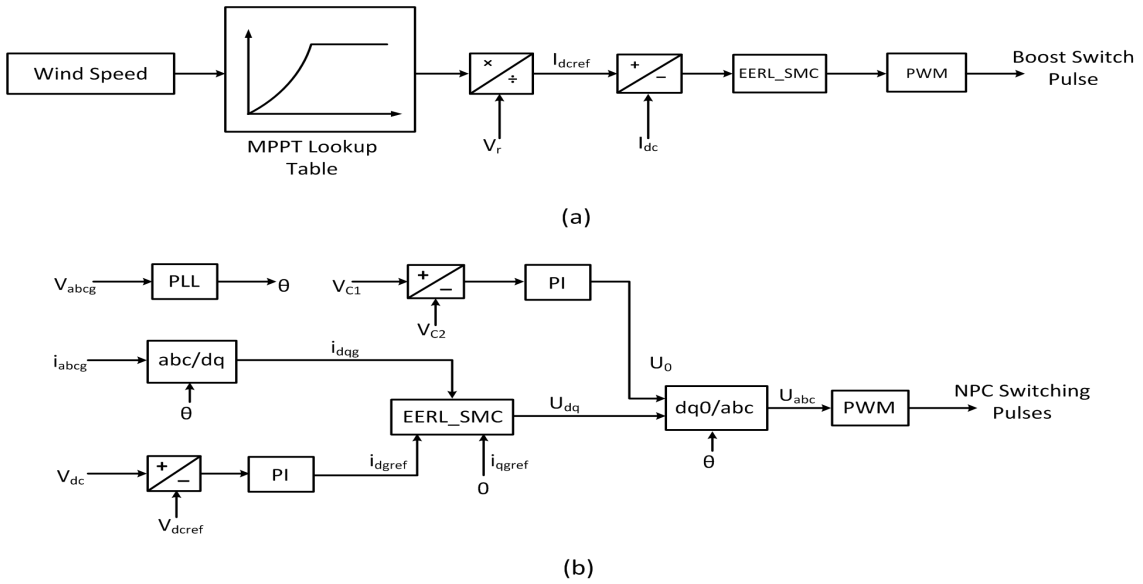

Fig. 4. SMC based EERL approach for: (a) Boost converter control, (b) NPC inverter control.

control of WECS. This implies that DC link voltage must be kept constant and regulated. Desired value of direct-axis current of grid is acquired by PI controller of DC link voltage.

V. Simulation and Experimental Results

A. Simulation Results of PMSG Wind Turbine

For verification of proposed control method in wind energy applications, simulation is performed by Matlab/Simulink. Characteristics of WECS and the proposed control parameters required for the simulation are detailed in Tables I and II of the Appendix.

The optimum value of TSR is $\lambda_{opt} = 6.37$; Therefore, the maximum value of power coefficient is $C_{p-max} = 0.4382$, calculated based on $\beta = 0°$ and λ_{opt}. Fig. 5(a) depicts $C_p(\lambda, \beta)$ using the values of Table II.

Using Eqs. (22), (32) and (33), a nonlinear function of β and V_ω is built. Therefore, an iterative nonlinear method can be adopted to solve it. Fig. 5(b) shows that how pitch angle adjusts when the wind speed varies.

It is worth noting that due to mechanical limitations in real systems, the pitch angle variation rate should be limited in the range from 3 to 10 $°/s$, based on the wind turbine size [40]. In order to perform simulation, wind speed profile shown in Fig. 5(c) has been utilized. We suppose that wind speed change rate is 3 m/s. In the simulation, rated wind speed is 15 m/s and we would like to examine WECS operation in regions II and III.

Power coefficient (C_p) of WECS associated with the wind profile is shown in Fig. 5(d). It can be seen that when the wind speed is lower than rated value, power coefficient of WECS is at C_{p-max}. This implies that the wind turbine is operating in MPPT mode. When the wind speed is higher than rated value, power coefficient is decreased to limit the generated power of WECS to the rated power of wind turbine.

The generated power of PMSG wind turbine and its speed are shown in Figs. 6(a) and 6(b). As it is seen, speed is

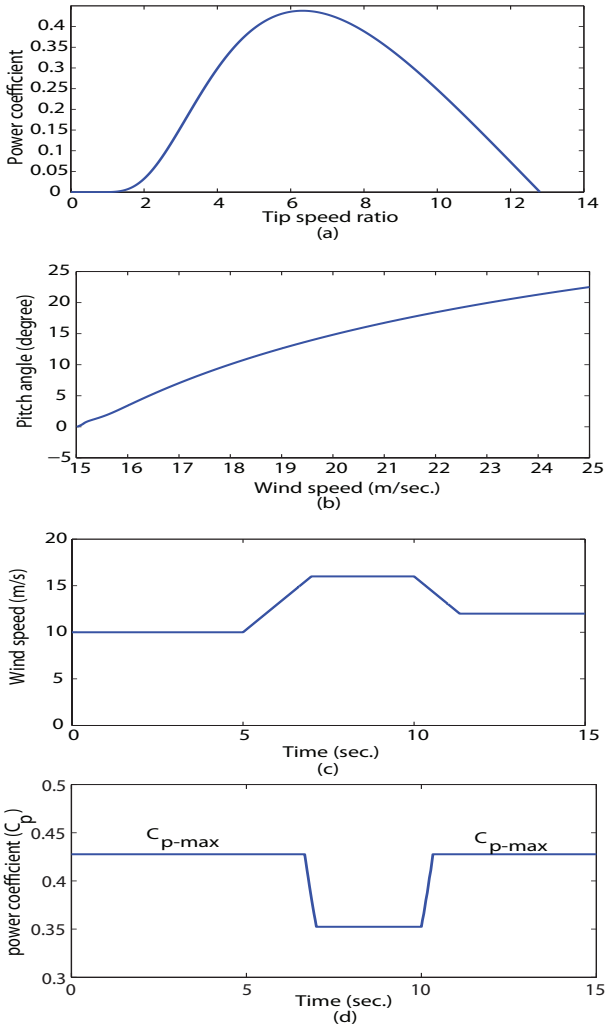

Fig. 5. Non electrical specifications of WECS. (a) C_p vs. TSR curve. (b) Pitch angle curve. (c) Wind profile. (d) C_p vs. time curve.

This article has been accepted for publication in a future issue of this journal, but has not been fully edited. Content may change prior to final publication. Citation information: DOI 10.1109/TIE.2016.2570718, IEEE Transactions on Industrial Electronics

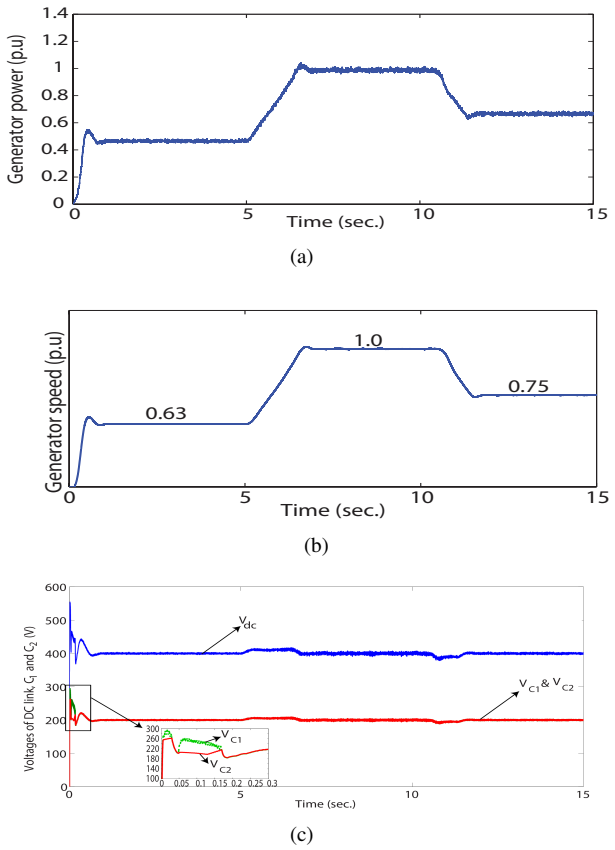

Fig. 6. Waveforms of: (a) PMSG power, (b) PMSG speed, and (c) DC link, C_1 and C_2 voltages.

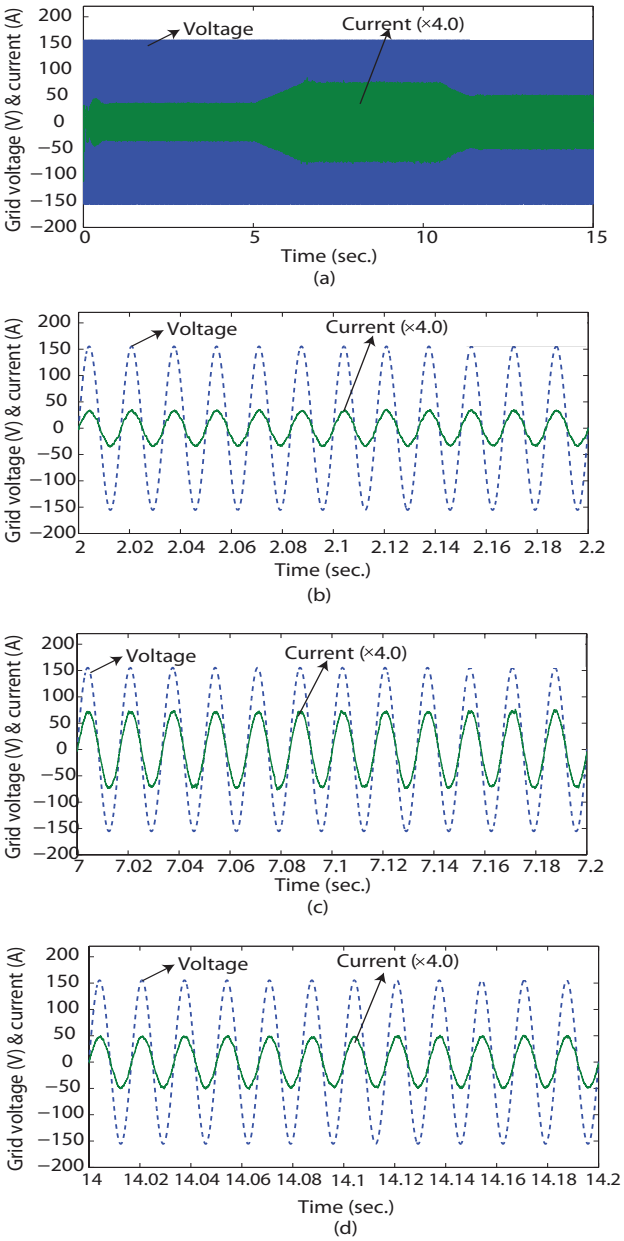

Fig. 7. Voltage and current waveforms of phase (a) at PCC in the ranges: (a) $0 \leq t \leq 15$, (b) $2 \leq t \leq 2.2$, (c) $7 \leq t \leq 7.2$, and (d) $14 \leq t \leq 14.2$.

increased when the wind speed goes up. As a result, electrical power generated by PMSG is increased. It is obvious that when wind speed goes down, speed and power of PMSG are reduced. At $v_\omega = 10$ and 12 m/s, which are less than rated wind speed, pitch angle is set to 0° to let the WECS extract all energy from wind. Clearly, PMSG power is less than nominal power of the system. In contrast, at $v_\omega = 16$ m/s, which is greater than rated wind speed, pitch controller modifies the pitch angle based on Fig. 5(b) to reduce the amount of power harvested by WECS, therefore; generator speed is controlled at its rated speed and 4 kW is generated by the wind turbine. Whereas the generator power is controlled by I_{dc}, their waveforms have the same shape characteristics.

Fig. 6(c) depicts waveforms of DC link voltage V_{dc} and DC link capacitors voltages V_{C_1} and V_{C_2}. DC link voltage has been greatly controlled to be kept constant at 400 V. When there is a change in wind speed, a small variation is observed in DC link voltage. As it is obvious, the controller regulates it very fast. As voltages of C_1 and C_2 can not be easily distinguished in Fig. 6(c), initial part of the figure is highlighted to show it clearly. After $t = 0.17$ s, capacitor voltages are balanced even in the presence of wind speed variation.

The target of grid-connected renewable energy system such as WECS is to transfer maximum power into the grid with UPF because poor power factor on the power network increases power line losses and makes it very difficult to keep the voltage regulated. Voltage and current waveforms of phase (a) at PCC as well as a closer observation of them are demonstrated in Fig. 7. It should be noted that current waveforms have been enlarged and multiplied by a constant to be seen more easily. One salient objective of the controller in WECS is to obtain unity power factor. From Fig. 7, it is clear that in steady state, current at the grid is in phase of voltage at all wind speeds. Since wind speed change rate is set at 3 m/s, there is no instantaneous variation of current at PCC. There exists UPF even during variation of wind speed.

Fig. 8 compares the chattering perspective of EERL and ERL methods. It is distinct that EERL method mitigates the chattering issue more than ERL approach.

This article has been accepted for publication in a future issue of this journal, but has not been fully edited. Content may change prior to final publication. Citation information: DOI 10.1109/TIE.2016.2570718, IEEE Transactions on Industrial Electronics

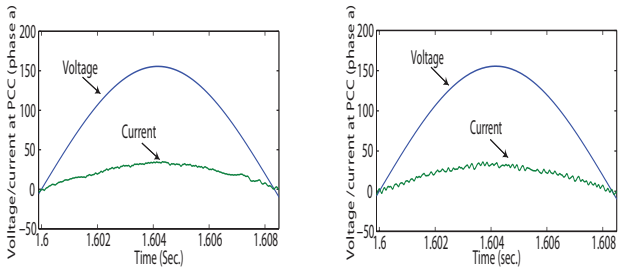

Fig. 8. Comparison of chattering issue of: (a) EERL method, and (b) ERL method.

One major impediment of diode rectifier in PMSG wind turbine is the high harmonic contents in the generator stator current which leads to the generator torque and DC link voltage ripples. Ripple in DC link voltage is smoothed by incorporating capacitor C_0 between diode rectifier and boost converter. Several studies have been directed to minimize the PMSG torque ripple connected to diode rectifier [10], [41]. Nonetheless, it must be devised to design the PMSG and related drive-train in such a way that they could tolerate generator torque ripple [20], [41]. Simulation results show that the maximum electromagnetic torque ripple of PMSG is approximately 0.17 per unit.

B. Experimental Results

For validation of proposed SMC based EERL method, a laboratory prototype according to Fig. 9 is implemented to evaluate proposed controller in which V_{dc} is a variable DC source. It should be noted this structure has been chosen for controller validation purpose due to the experimental limitations. Scheme used in Fig. 9 and applied controller can also be employed for grid integration of other types of renewable energy. By replacing the PMSG, MSC and DC bus with a DC source, DC link ripples are slightly ignored. Hence, voltage ripples of capacitors C_1 and C_2 are a little less than real system but the variation of DC link voltage is examined in the experiment along with the balancing challenge of the voltages V_{c1} and V_{c2}. In our set-up, clamping diodes and MOSFETs types are SCT2080KE and SCS220KG, respectively. dSPACE DS1103 real-time controller board is employed to implement the SMC based EERL with 20 μs sampling rate. This hardware encompasses a processor and some I/Os to be able to accomplish the control procedures. Real-Time Interface (RTI) of dSPACE lets us implement the Simulink and Stateflow models on the hardware. The experimental setup data is given in Table IV of the Appendix.

To explore the effectiveness of proposed method, it is compared with SMC based ERL and PI approaches. Fig. 10, 11 and 12 show the set-up results including the NPC inverter and L filter using EERL, ERL and PI approaches respectively in which V_{c1}, NPC output line voltage, and PCC voltage and current (phase a) are shown. Control parameters for EERL method are the same as parameters used in simulation, listed in Table III in the Appendix. For ERL approach, parameters

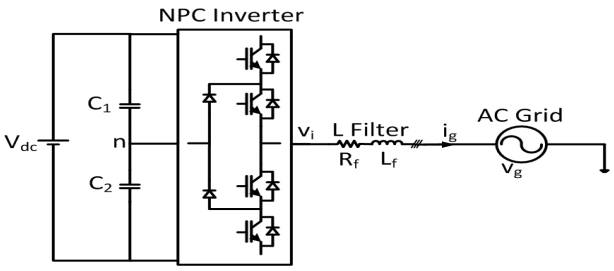

Fig. 9. Experimental set-up scheme.

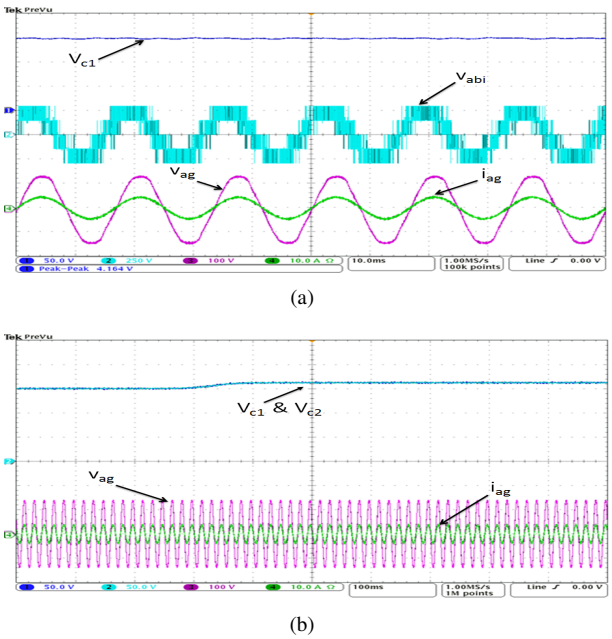

Fig. 10. Voltage of capacitor C_1, NPC voltage, and current and voltage waveforms of phase (a) at PCC using SMC based EERL in: (a) steady state mode, and (b) transient mode.

are as: $\alpha_d = \alpha_q = 0.1$, $\beta_d = \beta_q = 10$. Parameters associated with PI method are as: $K_p = 19.25$, $T_i = 0.01$ (current control), and $K_p = 0.95$, $T_i = 0.02$ (DC voltage control). These parameters are obtained such that we meet the requirements of settling time 1.2 $msec$ and overshoot 5.1 $\%$. Since a grid-connected NPC inverter is tested at this point, the main objectives are to reduce chattering phenomenon, to balance voltage of capacitors C_1 and C_2, to obtain UPF, and to achieve permissible harmonic level with low power losses and low switching frequency.

The five-level voltage waveform between phases (a) and (b) of the NPC inverter output, v_{abi} in Figs. 10(a), 11(a) and 12(a) demonstrate that the dynamic performance of the EERL approach is more smooth than the ERL and PI methods. Moreover, low voltage ripple of V_{C1} as well as voltage balancing depicted in these figures prove that the controller has been properly designed and applied to the system. Voltage of capacitor C_1 in all applied techniques is about 150 V, half of the DC link voltage ($V_{dc} = 300$ V). Figs. 10(b), 11(b) and 12(b) illustrate an increase of DC link voltage from 300V to 330V for three methods in which V_{C1} of EERL coincides with V_{C2} with lowest deviation and ripple during transients.

This article has been accepted for publication in a future issue of this journal, but has not been fully edited. Content may change prior to final publication. Citation information: DOI 10.1109/TIE.2016.2570718, IEEE Transactions on Industrial Electronics

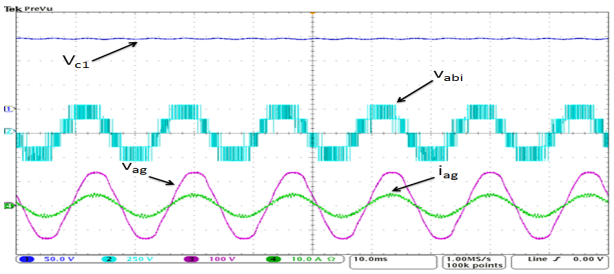

(a)

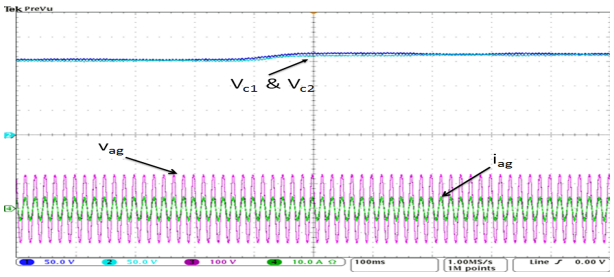

(b)

Fig. 11. Voltage of capacitor C_1, NPC voltage, and current and voltage waveforms of phase (a) at PCC using SMC based ERL in: (a) steady state mode, and (b) transient mode.

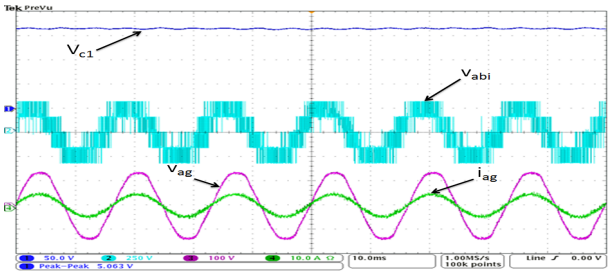

(a)

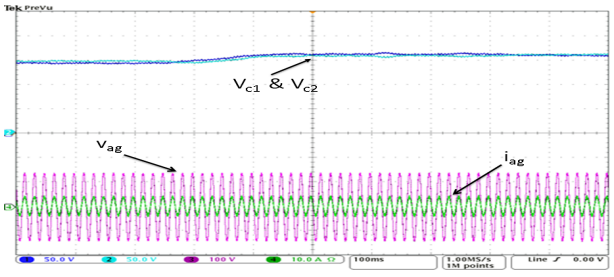

(b)

Fig. 12. Voltage of capacitor C_1, NPC voltage, and current and voltage waveforms of phase (a) at PCC using PI approach in: (a) steady state mode, and (b) transient mode.

In the IEEE standard for harmonic control in electrical power systems IEEE Std 519, allowable THD at PCC must be less than 5%. AMEC power analyzer has been used to capture voltage and current waveforms of the connection point to the grid to analyze THD of waveforms. Fig. 13 highlights one cycle of voltage and current at PCC. From Fig. 13, it is clear that all three methods have acceptable performance regarding THD of the current waveform. But it is observed that THD value obtained by EERL is 1.9% which is much smaller than THD of ERL method (3%) and PI approach (3.5%). It should be noted that by choosing aforesaid PI parameters for current controller, EERL outperforms PI method. Nevertheless, THD related to PI could be improved by selecting a smaller gain.

It is obvious that power factor in PI, ERL and EERL methods is almost 1 and therefore the reactive power injected to the grid through the NPC inverter is near zero. Power electronic converter designers consider the voltage ripple of DC link capacitors to be a key aspect in their design considerations. It can be deduced from experimental results that peak to peak voltage of capacitor is detracted by EERL method in comparison to ERL and PI methods.

Finally, to verify more the dynamic response of the SMC based EERL controller on the grid-tied NPC inverter in renewable energy applications considering input power variations, step changes in input power amplitude have been exerted to the set-up input. Fig. 14 shows the results for this case. Fig. 14(a) shows a decrease of DC link voltage from $330V$ to $290V$ and again up to $330V$, and Fig. 14(b) demonstrates step changes in current reference from $5A$ to $8A$.

It is evident that the proposed controller takes proper action in the short period of time to keep UPF operation throughout the working regions with different input powers, and to maintain the DC link voltage well-tracked its reference as well as to generate high quality power at PCC.

VI. Conclusion

In this paper, a sliding mode control based on enhanced exponential reaching law was proposed and investigated on the grid-connected PMSG wind turbine system. The examined topology consists of: diode rectifier, boost converter, NPC inverter and L filter. This topology can be used in low power and medium power wind turbine systems. Boost converter is controlled by maximum power point tracking idea of PMSG, while NPC inverter control is developed using the unity power factor concept. The key features of the proposed controller are: chattering minimization respect to conventional and exponential reaching law sliding mode controllers, proper voltage balancing performance of DC link capacitors, improving transient traits of WECS, and appropriate dynamic error tracking. The verification of the proposed reaching law for SMC approach was validated by both simulation and experiment.

This article has been accepted for publication in a future issue of this journal, but has not been fully edited. Content may change prior to final publication. Citation information: DOI 10.1109/TIE.2016.2570718, IEEE Transactions on Industrial Electronics

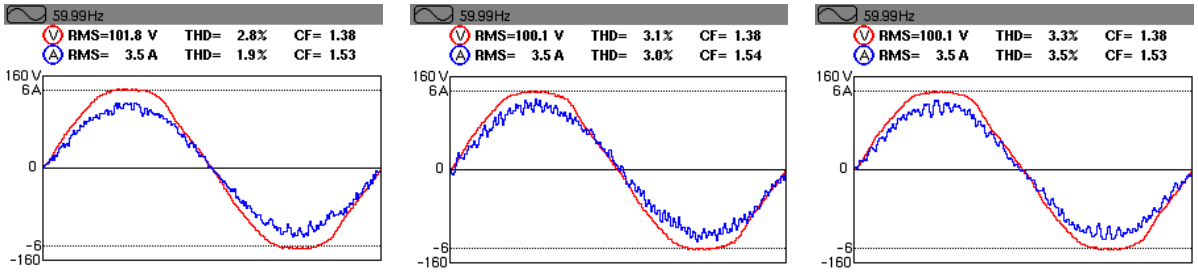

(a) (b) (c)

Fig. 13. Comparison of EERL, ERL and PI methods based upon THD of the currents injected to the grid: (a): EERL, (b): ERL, and (c): PI.

APPENDIX A

TABLE I
PMSG BASED WECS PARAMETERS

Characteristic	Symbol	Value
Air Density	ρ	1.225 kg/m^3
Blade Radius	R	1.2 m
Optimal Tip Speed Ratio	λ_{opt}	6.37
Max Power Coefficient	C_{p-max}	0.4382
Inertia	J	0.032 $kg.m^2$
Number of Poles	n_p	10
PMSG Resistance	R_s	0.135 Ω
PMSG Inductance	L_s	4 mH
PM Flux Linkage	λ_f	0.5 $V.s$
Rectifier Capacitance	C_0	1000 μF
Boost Inductance	L_{dc}	1.5 mH
DC Link Capacitance	C_1 and C_2	650 μF (each)
Filter Inductance	L_f	5 mH
Switching Frequency	f_{sw}	2 kHz
Grid Frequency	f	60 Hz
Grid Line Voltage	v_{ab}	$110\sqrt{3}$ V

TABLE II
COEFFICIENTS OF C_p

Coefficients	Value
c_1, c_2, c_3	0.22, 116, 0.5
c_4, c_5, c_6	0, 5, 12.5
c_7, x, β	0, 1.5, 0°

TABLE III
SMC BASED EERL PARAMETERS

Characteristics	Value
Λ_{dc}, Λ_d and Λ_q	75, 50, 50
K_{dc}, K_d and K_q	200, 150, 150
α_{dc}, α_d, α_q	0.3, 0.25, 0.25
β_{dc}, β_d and β_q	10, 5, 5
γ_{dc}, γ_d and γ_q	0.1, 0.1, 0.1

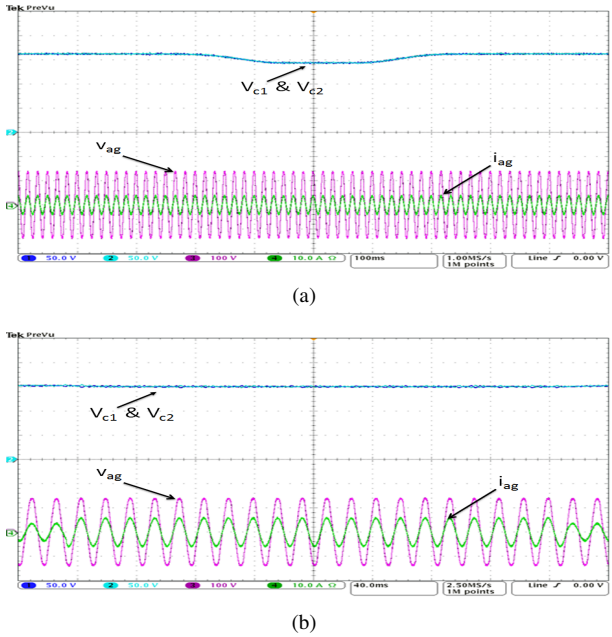

(a)

(b)

Fig. 14. Voltage and current waveforms at PCC: (a) V_{dc} alters in two level of voltages: 330V and 290V. (b) PCC reference current changes from 5A to 8A.

TABLE IV
EXPERIMENTAL SETUP PARAMETERS

Characteristics	Value
DC link voltage	300 V
C_1 and C_2	650 μF
L_f	5 mH
Switching frequency	2 kHz
Grid frequency	60 Hz
Grid line voltage	$100\sqrt{3}$ V

REFERENCES

[1] T. H. Nguyen and D. C. Lee, "Advanced fault ride-through technique for pmsg wind turbine systems using line-side converter as statcom," *IEEE Trans. Ind. Electron.*, vol. 60, no. 7, pp. 2842–2850, 2013.

[2] H. Mortazavi, H. Mehrjerdi, M. Saad, S. Lefebvre, D. Asber, and L. Lenoir, "Application of distance relay for distribution system monitoring," in *IEEE Power Energy Society General Meeting*, 2015, pp. 1–5.

[3] F. Blaabjerg, M. Liserre, and K. Ma, "Power electronics converters for wind turbine systems," *IEEE Trans. Ind. Applic.*, vol. 48, no. 2, pp. 708–719, 2012.

[4] H. Li and Z. Chen, "Overview of different wind generator systems and

their comparisons," *IET Ren. Pow. Gen.*, vol. 2, no. 2, pp. 123–138, 2008.

[5] M. Singh and A. Chandra, "Application of adaptive network-based fuzzy inference system for sensorless control of PMSG-based wind turbine with nonlinear-load-compensation capabilities," *IEEE Trans. Pow. Electron.*, vol. 26, no. 1, pp. 165–175, 2011.

[6] H. Vahedi and K. Al-Haddad, "Real-time implementation of a seven-level packed u-cell inverter with a low-switching-frequency voltage regulator," *IEEE Trans. Pow. Electron.*, vol. 31, no. 8, pp. 5967–5973, 2016.

[7] H. Vahedi, P. A. Labbé, and K. Al-Haddad, "Sensor-less five-level packed u-cell (puc5) inverter operating in stand-alone and grid-connected modes," *IEEE Trans. Ind. Inf.*, vol. 12, no. 1, pp. 361–370, 2016.

[8] F. Blaabjerg, "Future on Power Electronics for Wind Turbine Systems," *IEEE J. Emer. and Select. Topics in Pow. Electron.*, vol. 1, no. 3, pp. 139–152, 2013.

[9] M. Sharifzade, H. Vahedi, R. Portillo, M. Khenar, A. Sheikholeslami, L. Franquelo, and K. Al-Haddad, "Hybrid shm-she pulse amplitude modulation for high power four-leg inverter," *IEEE Trans. Ind. Electron.*, vol. PP, no. 99, pp. 1–1, 2016.

[10] C. Xia, Z. Wang, T. Shi, and Z. Song, "A novel cascaded boost chopper for the wind energy conversion system based on the permanent magnet synchronous generator," *IEEE Trans. Ener. Conv.*, vol. 28, no. 3, pp. 512–522, 2013.

[11] M. Iacchetti, G. Foglia, A. Di Gerlando, and A. Forsyth, "Analytical evaluation of surface-mounted pmsg performances connected to a diode rectifier," *IEEE Trans. Ener. Conv.*, vol. PP, no. 99, pp. 1–9, 2015.

[12] V. Yaramasu, B. Wu, M. Rivera, and J. Rodriguez, "A new power conversion system for megawatt pmsg wind turbines using four-level converters and a simple control scheme based on two-step model predictive strategy-part i: Modeling and theoretical analysis," *IEEE J. Emer. and Select. Topics in Pow. Electron.*, vol. 2, no. 1, pp. 3–13, 2014.

[13] T. R. de Freitas, P. J. MenegÃ¡z, and D. S. Simonetti, "Rectifier topologies for permanent magnet synchronous generator on wind energy conversion systems: A review," *Ren. and Sus. Ener. Reviews*, vol. 54, pp. 1334 – 1344, 2016.

[14] F. Delfino, F. Pampararo, R. Procopio, and M. Rossi, "A feedback linearization control scheme for the integration of wind energy conversion systems into distribution grids," *IEEE Sys. J.*, vol. 6, no. 1, pp. 85–93, 2012.

[15] Q. C. Zhong, Z. Ma, W. L. Ming, and G. C. Konstantopoulos, "Grid-friendly wind power systems based on the synchronverter technology," *Ener. Conv. and Manag.*, vol. 89, pp. 719–726, 2015.

[16] S. Li, T. A. Haskew, R. P. Swatloski, and W. Gathings, "Optimal and direct-current vector control of direct-driven PMSG wind turbines," *IEEE Trans. Pow. Electron.*, vol. 27, no. 5, pp. 2335–2337, 2012.

[17] A. Rajaei, M. Mohamadian, and A. Y. Varjani, "Vienna-Rectifier-Based Direct Torque Control of PMSG for Wind Energy Application," *IEEE Trans. Ind. Electron.*, vol. 60, no. 7, pp. 2919–2929, 2013.

[18] S. Muyeen and A. Al-Durra, "Modeling and control strategies of fuzzy logic controlled inverter system for grid interconnected variable speed wind generator," *IEEE Sys. J.*, vol. 7, no. 4, pp. 817–824, 2013.

[19] X. Yuan, F. Wang, D. Boroyevich, R. Burgos, and Y. Li, "DC-link voltage control of a full power converter for wind generator operating in weak-grid systems," *IEEE Trans. Pow. Electron.*, vol. 24, no. 9, pp. 2178–2192, 2009.

[20] B. Wu, Y. Lang, N. Zargari, and S. Kouro, *Power conversion and control of wind energy systems*. Hoboken, New Jersey: Wiley, 2011.

[21] M. Kuschke and K. Strunz, "Energy-efficient dynamic drive control for wind power conversion with pmsg: Modeling and application of transfer function analysis," *IEEE J. Emer. and Select. Topics in Pow. Electron.*, vol. 2, no. 1, pp. 35–46, 2014.

[22] L. Trilla, F. Bianchi, and O. Gomis-Bellmunt, "Linear parameter-varying control of permanent magnet synchronous generators for wind power systems," *IET Pow. Electron.*, vol. 7, no. 3, pp. 692–704, 2014.

[23] X. Hao, X. Yang, T. Liu, L. Huang, and W. Chen, "A sliding-mode controller with multiresonant sliding surface for single-phase grid-connected VSI with an LCL filter," *IEEE Trans. Pow. Electron.*, vol. 28, no. 5, pp. 2259–2268, 2013.

[24] G. Rigatos, P. Siano, and N. Zervos, "Sensorless control of distributed power generators with the derivative-free nonlinear kalman filter," *IEEE Trans. Ind. Electron.*, vol. 61, no. 11, pp. 6369–6382, 2014.

[25] K.-H. Kim, Y.-C. Jeung, D.-C. Lee, and H.-G. Kim, "Lvrt scheme of pmsg wind power systems based on feedback linearization," *IEEE Trans. Pow. Electron.*, vol. 27, no. 5, pp. 2376–2384, 2012.

[26] S.-K. Kim, H. Song, and J.-H. Lee, "Adaptive disturbance observer-based parameter-independent speed control of an uncertain permanent magnet synchronous machine for wind power generation applications," *Energies*, vol. 8, no. 5, p. 4496, 2015.

[27] W. Zhang, S. Gadsden, and S. Habibi, "Nonlinear estimation of stator winding resistance in a brushless dc motor," in *American Control Conference (ACC)*, 2013, pp. 4699–4704.

[28] Y. Shtessel, C. Edwards, L. Fridman, and A. Levant, *Sliding Mode Control and Observation*, ser. Control Engineering. New York, USA: Springer, 2013.

[29] F. Sebaaly, H. Vahedi, H. Y. Kanaan, N. Moubayed, and K. Al-Haddad, "Sliding-mode current control design for a grid-connected three-level npc inverter," in *International Conference on Renewable Energies for Developing Countries (REDEC)*, 2014, pp. 217–222.

[30] C. J. Fallaha, M. Saad, H. Y. Kanaan, and K. Al-Haddad, "Sliding-mode robot control with exponential reaching law," *IEEE Trans. Ind. Electron.*, vol. 58, no. 2, pp. 600–610, 2011.

[31] F. Valenciaga and P. Puleston, "High-Order Sliding Control for a Wind Energy Conversion System Based on a Permanent Magnet Synchronous Generator," *IEEE Trans. Ener. Conv.*, vol. 23, no. 3, pp. 860–867, 2008.

[32] W. Gao and J. C. Hung, "Variable structure control of nonlinear systems. A new approach," *IEEE Trans. Ind. Electron.*, vol. 40, no. 1, pp. 45–55, 1993.

[33] J. Slotine and W. Li, *Applied Nonlinear Control*. New Jersey, USA: Prentice Hall, 1991.

[34] V. Yaramasu and B. Wu, "Predictive control of three-level boost converter and npc inverter for high power pmsg-based medium voltage wind energy conversion systems," *IEEE Trans. Pow. Electron.*, vol. PP, no. 99, pp. 1–1, 2014.

[35] V. Yaramasu, B. Wu, S. Alepuz, and S. Kouro, "Predictive control for low-voltage ride-through enhancement of three-level-boost and npc-converter-based pmsg wind turbine," *IEEE Trans. Ind. Electron.*, vol. 61, no. 12, pp. 6832–6843, 2014.

[36] N. Orlando, M. Liserre, R. Mastromauro, and A. Dell'Aquila, "A survey of control issues in pmsg-based small wind-turbine systems," *IEEE Trans. Ind. Inf.*, vol. 9, no. 3, pp. 1211–1221, 2013.

[37] S. Muyeen, J. Tamura, and T. Murata, *Stability Augmentation of a Grid-connected Wind Farm*. London, UK: Springer, 2009.

[38] Z. Qiu, K. Zhou, and Y. Li, "Modeling and control of diode rectifier fed pmsg based wind turbine," in *4th International Conference on Electric Utility Deregulation and Restructuring and Power Technologies (DRPT)*, 2011, pp. 1384–1388.

[39] S. Heier, *Grid Integration of Wind Energy Conversion Systems*. New York, USA: Wiley, 1998.

[40] J. Slootweg, S. de Haan, H. Polinder, and W. Kling, "General model for representing variable speed wind turbines in power system dynamics simulations," *IEEE Trans. Pow. Sys.*, vol. 18, no. 1, pp. 144–151, 2003.

[41] Y. Xia, J. Fletcher, S. Finney, K. Ahmed, and B. Williams, "Torque ripple analysis and reduction for wind energy conversion systems using uncontrolled rectifier and boost converter," *IET Ren. Pow. Gen.*, vol. 5, no. 5, pp. 377–386, 2011.

Seyed Mehdi Mozayan received the B.S. and M.S. degree both in electrical engineering from K. N. Toosi University of Technology (KNTU), Tehran, Iran in 2002 and 2009, respectively. From 2004 to 2012, He also worked in oil, gas and petrochemical industries in which he had been involved in different projects associated with industrial power system. He is currently a Ph.D. candidate in the Department of Electrical Engineering, ÉTS, University of Quebec, Montreal, Canada. His main interests and experience include the wind turbine technology, electrical machine design, electrical machine drive, electric vehicle (EV), and renewable energy integration into the grid.

Maarouf Saad (M'04-SM'08) received a bachelor and a master degrees in electrical engineering from École Polytechnique of Montreal respectively in 1982 and 1984. In 1988, he received a Ph.D. from McGill University in electrical engineering. He joined École de technologie superieure in 1987 where he is teaching control theory. His research is mainly in nonlinear control and optimization applied to robotics and power systems.

Hani Vahedi (S'10) was born in Sari, IRAN, in 1986. He received his B.Sc. and M.Sc. degrees both in electrical engineering from K. N. Toosi University of Technology (KNTU), Tehran, IRAN in 2008 and Babol University of Technology, Babol, IRAN in 2011, respectively. He is currently pursuing his PhD at the École de Technologie Superieure (ÉTS), University of Quebec, in Montreal, Canada, as a member of Groupe de Recherche en Électronique de Puissance et Commande Industrielle (GRÉPCI). He is an active member of IEEE Industrial Electronics Society and its Student & Young Professionals committee. His research interests include power electronics multilevel converters topology, control and modulation techniques, power quality, active power filter, and their applications into smart grid, renewable energy conversion, UPS, battery chargers and electric vehicles.

Handy Fortin Blanchette (S'07-M'10) received the B.Eng., M.Eng., and Ph.D. degrees in electrical engineering from the École de Technologie Supérieure (ÉTS), Montreal, P.Q., Canada, in 2001, 2003, and 2010, respectively. From 1994 to 1997, he was engaged in industrial automation. From 1998 to 2000, he was with the Bombardier Transport-ÉTS Research Laboratory, Montreal, where he worked on a high power traction system. From 2001 to 2003, he was involved in the development of an electrical drive library for the Simulink (MATLAB) environment. From 2007 to 2010, he was with OPAL-RT Technologies, where he led CPU-based and FPGA-based power electronics real-time simulation projects. From 2010 to 2011, he was a Visiting Scholar at Center for Power Electronic and System, Virginia Polytechnic Institute and State University, Blacksburg, where he was involved in the packaging of high temperature converters for aircraft applications. He is presently an associate professor of Electrical Engineering at the École de Technologie Supérieure. His current research interests include EMI prediction, circuit modeling, and high density power converters packaging. He is a member of the IEEE.

Mohsen Soltani (S'05-M'08) received his M.Sc. degree in Electrical Engineering from Sharif University of Technology in 2004 and the Ph.D. degree in Electrical and Electronic Engineering from Aalborg University in 2008. He was a visiting researcher at Eindhoven University of Technology in 2007. He fulfilled a Postdoctoral and an Assistant Professor program at Aalborg University in 20008-2012. In 2010, he was granted a visiting scholar at Stanford University. He is an Associate Professor in the Department of Energy Technology at Aalborg University since 2012. During 2015, he completed a leadership training program by Harvard Business School. His research interests include modeling, control, optimization, estimation, fault detection and their applications to electromechanical and energy conversion systems, wind turbines, and wind farms. Some of his recent projects involve modeling, control, and estimation in large-scale wind farms and Model Predictive Control of wind turbines.